


Linear optical response from the odd-parity Bardasis-Schrieffer mode in locally non-centrosymmetric superconductors

Changhee Lee ^{1✉} & Suk Bum Chung ^{2,3✉}

On the recent report of a field-induced first order transition in the superconducting state of CeRh_2As_2 , which is a possible indication of a parity-switching transition of the superconductor, the microscopic physics is still under investigation. However, if two competing pairing channels of opposite parities do exist, a particle-particle collective mode referred to as the Bardasis-Schrieffer (BS) mode should generically exist below the pair-breaking continuum. The BS mode of the CeRh_2As_2 superconductor can couple to the light, as it arises from a pairing channel with the parity opposite to that of the superconducting condensate. Here, by using a generic model Hamiltonian we carry out a qualitative investigation on the excitation energy of the BS mode with respect to the out-of-plane magnetic fields and its contribution to the optical conductivity. Our findings indicate that the distinct coupling between the BS mode and the light can serve as evidence for the competing odd-parity channels of CeRh_2As_2 and other locally non-centrosymmetric superconductors.

¹Department of Physics and Astronomy, Seoul National University, Seoul 08826, Korea. ²Department of Physics and Natural Science Research Institute, University of Seoul, Seoul 02504, Korea. ³School of Physics, Korea Institute for Advanced Study, Seoul 02455, Korea. ✉email: changhee900820@gmail.com; sbchung0@uos.ac.kr

Discovering superconductors with odd-parity Cooper pairing has been a long-standing challenge in condensed matter physics, as they are rare in inversion symmetric solid-state systems. To name a few, UPt_3 ¹, UNi_2Al_3 ² and Sr_2RuO_4 ³ are the most notable candidates which have been suspected to host odd-parity Cooper pairings for a long time, though the case of a much studied candidate material Sr_2RuO_4 has grown more controversial in recent years^{4–8}.

Faced with this rarity of odd-parity superconducting materials, many researchers have endeavored to find realistic conditions favoring odd-parity superconductivity. For instance, the systems possessing a structural instability toward an inversion-symmetry-broken phase such as the pyrochlore oxide $\text{Cd}_2\text{Re}_2\text{O}_7$ drew attention for a potential to host an odd-parity superconducting phase^{9–12}.

Another mechanism for odd-parity superconductivity is suggested by a recent experiment on CeRh_2As_2 ^{13,14}. There a transition is observed when the external magnetic fields are applied along the c -axis within the superconducting phase of CeRh_2As_2 ¹³. According to the preceding theoretical studies^{15,16}, the transition referred to as the even-to-odd transition seems to occur between two superconducting phases of opposite parities under an inversion. The Pauli paramagnetic pair-breaking effect^{17,18} is a known mechanism for destroying the even-parity superconducting (eSC) phase. By contrast, an odd-parity superconducting (oSC) state can withstand the magnetic fields through an equal-(pseudo)spin pairing^{13,19–21}. It is noted that the combination of $P4/nmm$ nonsymmorphic crystal structure and the heavy-fermion characteristic supports strong intralayer Rashba-type spin-orbit couplings that are known to favor equal-(pseudo)spin pairings²⁰.

An intriguing implication of the even-to-odd transition in CeRh_2As_2 is the presence of competing pairing channels with opposite parities. The potential transition temperature $T_{c,o}$ of the oSC phase at zero field, which is preempted by the onset of the eSC phase in reality, is estimated to be close to the transition temperature $T_{c,e}$ of the eSC phase¹³. Moreover, phenomenological studies have reproduced the overall superconducting phase diagram in CeRh_2As_2 with comparable coupling strengths for both pairing channels^{13,22}.

Even if most of the theories set forth so far support that the high-field superconducting phase of CeRh_2As_2 is odd in parity, counter-arguments have also been raised. For instance, a theoretical study proposed that the observed magnetic field-induced phase transition arises not from the parity switching of the superconducting gap but from the spin-flipping in the coexistent antiferromagnetic order parameter²³. Therefore, further experimental signatures need to be sought for the first-order transition that switches the parity of the superconducting gap. Of the many ways to find indisputable evidence for the symmetry of the superconducting phase, one is to investigate the collective modes in the superconducting phase²⁴. Historically, the detection of a number of the nearly degenerate collective modes in the superfluid B -phase of ^3He proved to be the decisive evidence in favor of the spin-triplet pairing²⁵.

In this regard, we note that, if the first order transition is really associated with the parity-switching transition, $T_{c,o} \approx T_{c,e}$ not only implies the close competition between two pairing channels of opposite parities but also provides a favorable condition for a collective mode, known as the Bardasis-Schrieffer (BS) mode²⁶, to appear far from the pair-breaking continuum. The BS mode is an exciton-like collective mode in superconductors due to an uncondensed pairing channel and indicates an instability towards another superconducting phase breaking some symmetries of the superconducting ground state. As a precursor of the instability of the superconducting ground state, the BS mode softens as the uncondensed channel gets stronger so that the competition between the uncondensed pairing channel and the condensed

pairing channel defining the superconducting ground state is enhanced. However, such closely competing pairing channels have rarely been found in superconductors, with one of a few exceptions being the iron-based superconductors, where the close competition between the s -wave and d -wave pairing channels has been confirmed by the Raman detection of the BS mode^{27–30}.

Besides the possible existence of the BS mode, it is worth noting that the collective mode can possess a non-zero optical coupling when the parity of the uncondensed pairing channel under inversion is the opposite of that of the superconducting ground state³¹. This feature makes the detection of the collective mode possible through the optical response in the linear response regime, which can be thought of as compelling proof for the existence of a strong odd-parity pairing channel. This is in sharp contrast to the Fe-based superconductors where the electronic Raman spectroscopy is used to detect the BS mode from the d -wave channel as this pairing channel and the s -wave ground state pairing share the same parity^{27,28,32–34}. Thus, in the case of CeRh_2As_2 , the detection of the BS mode would be conclusive evidence for the occurrence of parity-switching at the observed transition between the two superconducting phases.

In this work, we conduct a qualitative study on the BS modes in the clean limit superconducting phase of a locally non-centrosymmetric system such as CeRh_2As_2 , which arise from the odd-parity and even-parity pairing channel in the eSC state and oSC state, respectively. First, we demonstrate the even-to-odd parity transition by the Pauli paramagnetic effect at the zero-temperature at the level of a mean-field description. We then briefly introduce the generalized random phase approximation (GRPA)^{35,36} which provides the basis of the analysis in this work. Also, it is shown that the BS mode from the uncondensed pairing channel can be linearly coupled to the light. This is ascribed to the origin of the BS mode whose parity is opposite to the condensed Cooper pairs. Using the GRPA, we investigate the softening of the BS modes under the external magnetic fields along the c -axis and its contribution to the optical conductivity.

Results

Mean-field analysis of the even-to-odd transition. We start our presentation by demonstrating the field-induced even-to-odd transition in the superconducting phase in a locally non-centrosymmetric layered structure by using a mean-field description at the zero-temperature. For results valid in a wider range of temperature and magnetic fields, we refer to refs. 15,16,21,37.

To describe the normal phase of the representative locally non-centrosymmetric system, CeRh_2As_2 , with the point group D_{4h} , we use a model Hamiltonian given by refs. 13,16,20,21:

$$H_0(\mathbf{k}) = \sum_{i=0}^2 \varepsilon_{i0}(\mathbf{k})\sigma_i + \sum_{i=1}^3 \varepsilon_{3i}(\mathbf{k})\sigma_3s_i - \mu \quad (1)$$

with

$$\varepsilon_{00}(\mathbf{k}) = 2t(2 - \cos k_x - \cos k_y), \quad (2)$$

$$\varepsilon_{10}(\mathbf{k}) = t_{c,1} \cos \frac{k_z}{2} \cos \frac{k_x}{2} \cos \frac{k_y}{2}, \quad (3)$$

$$\varepsilon_{20}(\mathbf{k}) = t_{c,2} \sin \frac{k_z}{2} \cos \frac{k_x}{2} \cos \frac{k_y}{2}, \quad (4)$$

$$\varepsilon_{31}(\mathbf{k}) = -\alpha_R \sin k_y, \quad (5)$$

$$\varepsilon_{32}(\mathbf{k}) = \alpha_R \sin k_x, \quad (6)$$

$$\varepsilon_{33}(\mathbf{k}) = \lambda_1 \sin k_z \sin k_x \sin k_y (\cos k_x - \cos k_y), \quad (7)$$

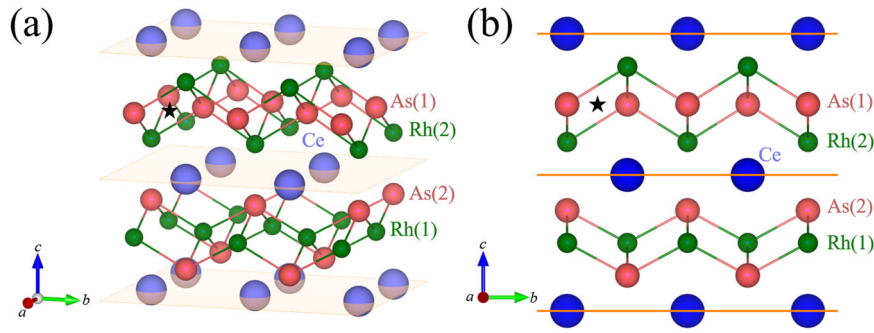


Fig. 1 Crystal structure of CeRh_2As_2 . **a** Bird's eye view of the structure. **b** A view from the (100) direction. An inversion center is marked by a black star.

where σ_i and s_i are the Pauli matrices for the orbital and spin degrees of freedom, respectively. The eigenenergies ξ_i and eigenvectors $|i, \pm\rangle$ of H_0 for $i=1,2$ can be found in the subsection “Microscopic model” in the “Methods” section.

Note that two orbital degrees of freedom should be introduced to take account of the locally non-centrosymmetric feature of the system. The reason is easily understood by looking into the crystal structure of CeRh_2As_2 ³⁸. In Fig. 1a, the crystal structure is depicted with three {001} lattice planes composed of Ce atoms. The locally broken inversion symmetry around Ce atoms is easily noted in Fig. 1b where the crystal structure is viewed from the (100) direction. Still, there is a global inversion symmetry whose center is marked by the black star in Fig. 1, under which no individual atom is left invariant. This global inversion is represented by $\mathcal{P} = \sigma_1 s_0$ in the basis of the model Hamiltonian $H_0(\mathbf{k})$ in Eq. (1).

$t_{c,1}$ and $t_{c,2}$ are the hoppings between the nearest-neighbor Ce layers depicted in Fig. 1. These hoppings endow the three-dimensional characteristics of the electronic structure. α_R and λ_I denote the intra-layer Rashba- and inter-layer Ising-type spin-orbit couplings, respectively. Note that the sign of the Rashba spin-orbit coupling alternates layer-by-layer, which reflects the locally non-centrosymmetric structure of the system shown in Fig. 1b.

Throughout this work, we ignore λ_I since this spin-orbit coupling corresponds to a spin-dependent inter-layer hopping between the two next-nearest-neighboring layers, and thus it is expected to be much weaker than the spin-independent inter-layer hoppings $t_{c,1}$ and $t_{c,2}$ between the nearest layers and the intra-layer Rashba spin-orbit coupling α_R .

In addition, we assume that the Rashba-type spin-orbit coupling α_R is much larger than the inter-layer hoppings $t_{c,1}$ and $t_{c,2}$ following refs. 13,20. In this limit of large Rashba spin-orbit coupling, the difference between $t_{c,1}$ and $t_{c,2}$ has no significant effect on the band structure except for a weak modulation of the Fermi surface along the k_z -axis. Thus, $t_c \equiv t_{c,1} = t_{c,2}$ is assumed throughout this work.

With this lattice model, we consider two spin-singlet pairing channels whose form factors are represented by σ_0 and σ_z . These are used to reproduce the magnetic field-temperature (H - T) phase diagram of CeRh_2As_2 in refs. 13,20,21,37. The pairing channel represented by σ_0 describes a uniform s -wave pairing. Meanwhile, σ_z represents a pairing channel whose sign alternates layer-by-layer, in which way the two orbital degrees of freedom endow it with the odd parity with respect to the global inversion despite being singlet in the physical spin sector. Hence, we call the superconducting state, where the pairing channel σ_0 is condensed while σ_z is uncondensed, the eSC state. The opposite case is called the oSC state. Throughout this paper, we use for conciseness the nomenclature p SC state with $p = e, o$ for the eSC and the oSC, respectively, and $p = n$ for the normal state.

The Bogoliubov-de Gennes (BdG) Hamiltonian for the p SC state including the Zeeman term $\mathbf{B} \cdot \mathbf{s}$ is given by

$$H_{\text{BdG}}^{(p)}(\mathbf{B}, \mathbf{k}) = \tau_0 \mathbf{B} \cdot \mathbf{s} + \tau_z H_0(\mathbf{k}) + \Delta_p \tau_x^{(p)}, \quad (8)$$

with $\tau_i^{(e)} = \tau_i \sigma_0$ and $\tau_i^{(o)} = \tau_i \sigma_z$ for $i = x, y, z$. Here, the basis field operator of the BdG Hamiltonian is $\hat{\Psi}_{\mathbf{k}} = (\hat{C}_{\mathbf{k}}, \hat{C}_{-\mathbf{k}}^\dagger(i s_y))^\top$ ^{39,40}. The magnetic field along (perpendicular to) the c -axis in Fig. 1 is denoted by $B_z(B_x)$ and it is referred to as the out-of-plane (in-plane) magnetic field in this work. The gap amplitude Δ_p , presumed to be real, is determined from the gap equation:

$$\Delta_p = \frac{g_p}{2} \sum_{\mathbf{k}} \text{Tr} \left[\tau_x^{(p)} G_{\mathbf{k}}^{(p)} \right], \quad (9)$$

with $G_{\mathbf{k}}^{(p)} = i\omega - H_{\text{BdG}}^{(p)}(\mathbf{k})$, while $\Delta_{\bar{p}} = 0$ where \bar{p} denotes the uncondensed pairing channel in the p SC state. Here, $\sum_{\mathbf{k}} = (\beta V)^{-1} \sum_{\mathbf{k}}$ is the normalized summation over a pair of Matsubara frequency and the three-dimensional momentum $\mathbf{k} = (i\omega, \mathbf{k})$, where $\beta = 1/k_B T$ and V are the inverse of the temperature and the volume of the system, respectively. The coupling constants g_e and g_o are assumed to be constant for the simplicity of the presentation. This assumption is valid in the weak-coupling regime which is suitable for the qualitative study.

Though both pairing channels are spin-singlet pairings, the Pauli paramagnetism through the Zeeman term can induce an even-to-odd phase transition which can be shown by comparing the zero-temperature (Gibbs) free energies of eSC and oSC phases

$$F_p(B_z) = \frac{\Delta_p^2}{4g_p} + \sum_{\mathbf{k}} \frac{\text{Tr} [H_0(\mathbf{k}) - \sum_n E_n^{(p)}(B_z, \mathbf{k})]}{2}. \quad (10)$$

Here, $E_n^{(p)}(B_z, \mathbf{k})$ ($n = 1, 2$) denotes a positive branch of the eigenvalues of the BdG Hamiltonian $H_{\text{BdG}}^{(p)}(B_z, \mathbf{k})$ and $\sum_{\mathbf{k}} \equiv V^{-1} \sum_{\mathbf{k}}$. Figure 2a illustrates the free energies $\delta F_p(B_z) \equiv F_p(B_z) - F_n(0)$ of the p SC state from which the zero-field normal phase free energy is subtracted. The parameters used are written in the caption of Fig. 2. The qualitative features of the system are well displayed with this set of parameters. g_e is chosen so that $\Delta_e = 0.004$ is obtained by Eq. (9), which is used throughout this work unless otherwise noted.

Each curve in Fig. 2a is well described by

$$F_p(B_z) = F_p(0) - \frac{1}{2} \chi_{\text{spin}}^{(p)} B_z^2, \quad (11)$$

where $\chi_{\text{spin}}^{(p)}$ is the spin susceptibility of the p SC state. The crossing point at the Pauli-limiting field $B_{z,p}$ between the normal (black dashed line) and eSC (black line) phases marks a first-order transition between the normal and eSC phase. Using Eq. (11), $B_{z,p}$

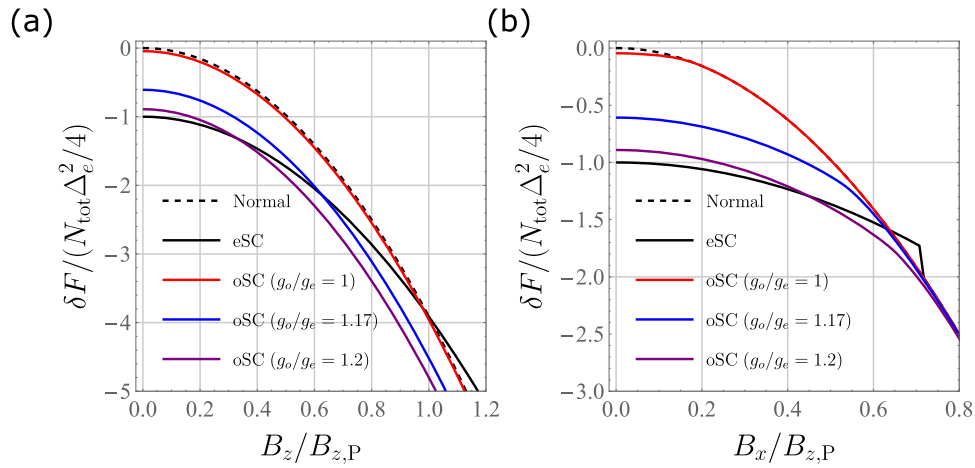


Fig. 2 Magnetic field dependence of free energies of the normal state, even-parity and odd-parity superconducting states. **a** Free energies versus the out-of-plane magnetic field B_z along the c -axis. **b** Free energies under the in-plane magnetic field B_x . Both magnetic fields are normalized by the Pauli limiting field $B_{z,P}$. The dashed line, and the black solid line depict the free energy of the normal state, and the even-parity superconducting state, respectively. The red, blue, and magenta lines correspond to the free energies of the odd-parity superconducting state for $g_o/g_e = 1, 1.17, 1.2$, respectively, where g_e and g_o are the coupling strengths for the even-parity pairing channel and the odd-parity pairing channel introduced in Eqs. (9) and (13). The parameters $t = 2$, $\mu = 0.5$, $t_{c,1} = t_{c,2} = 0.1$, $\alpha_R = 0.34$ and $\Delta_e = 0.004$ are used.

is given by

$$B_{z,P} = \sqrt{\frac{F_n(0) - F_e(0)}{(\chi_{\text{spin}}^{(n)} - \chi_{\text{spin}}^{(e)})/2}}. \quad (12)$$

Compared to the conventional Pauli-limiting critical field referred to as the Chandrasekhar-Clogston field $B_{z,CC} = \sqrt{2\{F_n(0) - F_e(0)\}/\chi_{\text{spin}}^{(n)}}$, $B_{z,P}$ is several times larger because of the non-vanishing $\chi_{\text{spin}}^{(e)}$ due to the sizable Rashba spin-orbit couplings^{15,41}.

The red, blue, and green lines in Fig. 2b denote the free energies of the oSC states with $g_o = g_e$, $g_o = 1.17g_e$ and $g_o = 1.2g_e$, respectively. Since $\chi_{\text{spin}}^{(o)} = \chi_{\text{spin}}^{(n)}$ as shown in Fig. 2a, a transition due to the Pauli paramagnetic depairing does not occur between the normal phase and the oSC state. The crossing point between the free energies of the eSC state and the oSC state for a given g_o indicates the even-to-odd transition observed in the experiment¹³. Moreover, the slopes of the lines are different at the crossing point, which means the transition is of the first order and the magnetization changes discontinuously at the transition.

Note that eSC state can be more stable than the oSC state at zero fields even if $g_o > g_e$, because the inter-layer spin-independent hoppings ε_{10} and ε_{20} effectively weaken the odd-parity pairing channel. For example, with the aforementioned parameters, we obtain 1.21 for the critical ratio $r_c \equiv g_{o,c}/g_e$ at which the eSC and oSC states degenerate at zero fields. Above the critical ratio, the oSC state is the superconducting ground state of the system at zero field. In the two-dimensional limit in which the ratio $\alpha_R/\max(|t_{c,1}|, |t_{c,2}|)$ is infinite, the electrons do not discern the trivial gap function σ_0 from the sign-alternating gap function σ_z , and thus $r_c \rightarrow 1$.

Though the effect of the out-of-plane magnetic fields is of main interest, we present the free energies under the in-plane magnetic fields as well. Figure 2b displays the free energies of the normal and superconducting phases under in-plane magnetic fields B_x . The free energies of the normal and the eSC phase cross at the Pauli-limiting in-plane magnetic field $B_{x,P}$ which is smaller than $B_{z,P}$, and this is consistent with the experiment^{13,42}. When it comes to the oSC state, we do not see a first-order transition to the normal phase due to the Pauli depairing, while an exponential

decrease of the gap function is seen with the increasing in-plane magnetic fields. (See Supplementary Note 1 for more details).

Furthermore, the critical in-plane magnetic field at which the oSC state and the eSC state degenerate is very close to $B_{x,P}$ for a fair range of g_o/g_e . As a result, up to the impurity and the finite-temperature effect, it can be challenging to detect the oSC state which would appear between the eSC and the normal phases. This is consistent with the experimental result where a phase transition into the oSC state by the in-plane magnetic field is not detected¹³.

Effective action for the pairing fluctuation. To study the BS mode, we use the generalized random phase approximation (GRPA)^{26,35,36,43}, which is one of the primary methods to incorporate the effect of the collective modes in the superconducting phase. Before applying the method to our case, we first briefly introduce the formulation of the GRPA.

Concerned with the linear optical response of the fluctuation from the uncondensed pairing channels around the (meta)stable superconducting condensate, we consider an attractive electronic interaction consistent with the gap equation in Eq. (9):

$$\hat{V} = -\frac{1}{2} \sum_p \sum_{k_1, k_2, q} g_p \hat{\Pi}_p(k_1, k_1 - q) [\hat{\Pi}_p(k_2, k_2 - q)]^\dagger, \quad (13)$$

where $\hat{\Pi}_p(k_1, k_2) = \hat{\Psi}_{k_1}^\dagger \tau_{\pm}^{(p)} \hat{\Psi}_{k_2}$ with $\tau_{\pm}^{(p)} = (\tau_x^{(p)} \pm i\tau_y^{(p)})/2$. \sum_p is the summation over the pairing channels represented by σ_0 and σ_z . We generally expect $g_o \neq g_e$; one simplest case being the combination of the on-site attractive interaction and the pair hopping interaction between the Ce atoms on the neighboring layer. Other pairing channels such as those discussed in refs. 21,41 do not couple linearly to the light because of the symmetries of H_0 with negligible λ_1 as shown in the subsection ‘‘Other odd-parity channels’’ in the ‘‘Methods’’ section.

After adding \hat{V} to the normal phase action $S_0 = \frac{1}{2} \sum_k \hat{\Psi}_k^\dagger (i\omega - H_0) \hat{\Psi}_k$, we obtain the effective action for the pairing fluctuations under external electromagnetic fields in the p SC state through the standard procedure in the functional integral approach (see subsection ‘‘Macroscopic model’’ in the

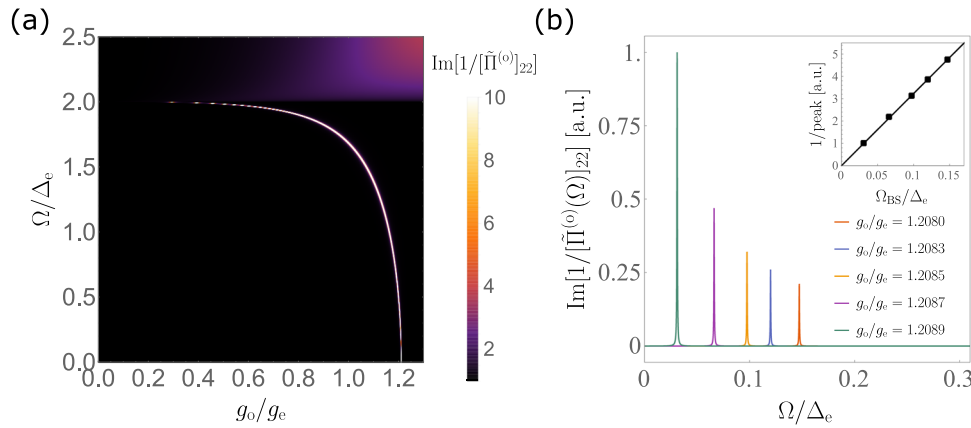


Fig. 3 The spectral function $\text{Im}[1/[\tilde{\Pi}^{(o)}]_{22}]$ of the Bardasis-Schrieffer (BS) mode. $[\tilde{\Pi}^{(o)}]_{22}$ is the propagator of the BS mode introduced in Eq. (16). **a** False color plot of the spectral function of the BS mode in the g_o/g_e – Ω plane. **b** The spectral function versus the frequency for the ratios g_o/g_e close to the critical ratio -1.21 at which the BS mode becomes gapless as shown in (a). g_e and g_o are the coupling strengths for the even-parity pairing channel and the odd-parity pairing channel introduced in Eq. (9) and Eq. (13). Δ_e is the magnitude of the superconducting gap function in the even-parity superconducting state. Ω_{BS} , which is referred to as the gap of the BS mode in the main text, denotes the frequency where the peak of the spectral function is located. The inverse of the height of each peak is linearly dependent on Ω_{BS} as shown in the inset.

“Methods” section):

$$\mathcal{S}_{\text{eff}}^{(p)} = \frac{1}{2} \sum_{\Omega} (\mathcal{A}_0, \eta_a^{(p)})_{-i\Omega} \Lambda_p(i\Omega) \begin{pmatrix} \mathcal{A}_0 \\ \eta_b^{(p)} \end{pmatrix}_{i\Omega} + \frac{1}{2} \sum_{\Omega} (\mathcal{A}_i, \eta_a^{(p)})_{-i\Omega} \Lambda_{\bar{p}}(i\Omega) \begin{pmatrix} \mathcal{A}_j \\ \eta_b^{(p)} \end{pmatrix}_{i\Omega}. \quad (14)$$

The auxiliary bosonic fields $\eta_a^{(p)}$ with $a=1,2$ are introduced through the Hubbard–Stratonovich transformation. Associated with $\tau_a^{(p)}$, they represent the real and imaginary parts of the fluctuation in the condensed pairing channel, respectively. Importantly, they correspond to the amplitude and the phase fluctuation, respectively, when Δ_p is real. $\eta_a^{(p)}$ with $a=1,2$ associated with $\tau_a^{(p)}$ represent the fluctuations in the uncondensed pairing channel. The electromagnetic four-potential $\mathcal{A}_\mu = |e|(-iA_0, \mathbf{A})$ is defined by multiplying the unit charge $|e|$ to the conventional four-potential for conciseness. Note that we omit the momentum \mathbf{q} dependence of η and \mathcal{A} since the London limit ($\mathbf{q} \rightarrow \mathbf{0}$) of the linear response is our interest.

The kernels Λ_p and $\Lambda_{\bar{p}}$ in Eq. (14) are given as

$$\Lambda_p = \begin{pmatrix} K_{00} & L_{0b}^{(p)} \\ R_{a0}^{(p)} & \tilde{\Pi}_{ab}^{(p)} \end{pmatrix}, \quad \Lambda_{\bar{p}} = \begin{pmatrix} K_{ij} & L_{ib}^{(p)} \\ R_{aj}^{(p)} & \tilde{\Pi}_{ab}^{(p)} \end{pmatrix}, \quad (15)$$

where the frequency dependence is omitted for conciseness (See the subsection “Macroscopic model” in the “Methods” section for the definition of the sub-blocks in Eq. (15)). The real-frequency kernels are obtained by the analytical continuation $i\Omega \rightarrow \Omega^+ = \Omega + i\epsilon$. $\epsilon = 10^{-6} = 2.5 \times 10^{-4} \Delta_e$ is used throughout this work unless otherwise noted.

Note that the effective actions $\mathcal{S}_{\text{eff}}^{(p)}$ for $p=e$ and $p=o$ are decomposed into two groups involving Λ_p and $\Lambda_{\bar{p}}$. This is because of the global inversion symmetry $\tau_0 \mathcal{I}$ ($\tau_z \mathcal{I}$) of the BdG Hamiltonian of the eSC (oSC) state. Also, Eqs. (14) and (15) explicitly show that the fluctuations of the uncondensed channel are involved in the optical response in the second block $\Lambda_{\bar{p}}$ in Eq. (15).

It also deserves to be noted that the effect of vortices in type-II superconductors is ignored since the critical fields $H_{c,2}$ of the eSC and oSC are about four times higher than the critical field for the even-to-odd transition¹³ which is our main focus.

Bardasis-Schrieffer mode at zero field. Given the effective action $\mathcal{S}_{\text{eff}}^{(p)}$, we study the BS mode originating from the fluctuations $\eta_1^{(p)}$ and $\eta_2^{(p)}$ in the uncondensed pairing channel^{25,26,28,43,44}. The equation of motion for the BS mode is given by $0 = \delta \mathcal{S}_{\text{eff}}^{(p)} / \delta \eta^{(p)}$ which is rearranged into

$$\eta^{(p)} = -[\tilde{\Pi}^{(p)}]^{-1} R^{(p)} \mathcal{A}, \quad (16)$$

where $\tilde{\Pi}^{(p)}(\Omega)$ is the propagator of the fluctuations $\eta^{(p)} = (\eta_x^{(p)}, \eta_y^{(p)})$. Since the BS mode arises from this fluctuation, the gap of the mode can be obtained by finding the singularity of the right-hand side (RHS) in Eq. (16) by solving $\det[\tilde{\Pi}^{(p)}] = 0$, which is denoted by Ω_{BS} throughout this work.

To figure out the physical implication of the BS mode, we analyze $\tilde{\Pi}^{(o)}$ based on our numerical and analytical results for the eSC state. As shown in Supplementary Note 2, $[\tilde{\Pi}^{(o)}(\Omega)]_{12}$ and $[\tilde{\Pi}^{(o)}(\Omega)]_{21}$ are vanishingly small, and $[\tilde{\Pi}^{(o)}(\Omega)]_{11}$ are finite for $|\Omega| < 2\Delta_e$. Thus, the zero of $\det[\tilde{\Pi}^{(o)}(\Omega)] \approx [\tilde{\Pi}^{(o)}(\Omega)]_{11} [\tilde{\Pi}^{(o)}(\Omega)]_{22}$ is largely identical to the zero of $[\tilde{\Pi}^{(o)}(\Omega)]_{22}$ which can be understood as the propagator of the BS mode, and Ω_{BS} can be found by looking into the singular peak of the spectral function $\text{Im}[1/[\tilde{\Pi}^{(o)}(\Omega)]_{22}]$. Figure 3a shows the spectral function $\text{Im}[1/[\tilde{\Pi}^{(o)}(\Omega)]_{22}]$ of the BS mode versus g_o/g_e in the eSC state at zero field. The gap of the BS mode Ω_{BS} is clearly identified. Increasing g_o/g_e drops Ω_{BS} , and Ω_{BS} becomes zero at the critical ratio $r_c = g_{o,c}/g_e \sim 1.21$. For larger g_o/g_e , the BS mode disappears, which is consistent with the free-energy analysis through the mean-field calculation.

To relate the gap of the BS mode Ω_{BS} to the stability of the superconducting condensate against the condensation of the other pairing channel, we first derive a semi-analytical expression for Ω_{BS} which is given by

$$\frac{2y \arcsin y}{\sqrt{1-y^2}} = \frac{1}{g_o N_{\text{tot}}} \langle \sin^2 \chi \rangle_{\text{FS}} - \frac{1}{g_e N_{\text{tot}}} \quad (17)$$

$$= -\ln \frac{T_{c,o}}{T_{c,e}}, \quad (18)$$

where $y = \Omega_{\text{BS}}/2\Delta_e$, $\sin \chi = \sqrt{\varepsilon_{31}^2(\mathbf{k}) + \varepsilon_{32}^2(\mathbf{k})} / \sqrt{\varepsilon_{10}^2(\mathbf{k}) + \varepsilon_{20}^2(\mathbf{k}) + \varepsilon_{31}^2(\mathbf{k}) + \varepsilon_{32}^2(\mathbf{k})}$, and $N_{\text{tot}} = N_1 + N_2$ with

$N_{i=1,2}$ being the density of states of the i -th Fermi surface given by $\xi_i = 0$. [The total density of states is $2N_{\text{tot}}$ due to the Kramers' degeneracy]. Here, $\langle \cdots \rangle_{\text{FS}} = \sum_{i=1}^2 N_i \langle \cdots \rangle_{\text{FS},i} / (N_1 + N_2)$ with $\langle \cdots \rangle_{\text{FS},i}$ being the angular average over the i th Fermi surface (for the derivation, see the subsection "Relation between the critical temperatures and BS mode gap" in the "Methods" section). In the second line, the weak-coupling formulae of the superconducting transition temperature T_c for the eSC state and the preempted oSC state are used, which are given by $g_e N_{\text{tot}} = -1/\ln(T_{c,e}/\Lambda)$ and $\langle \sin^2 \chi \rangle_{\text{FS}} g_o N_{\text{tot}} = -1/\ln(T_{c,o}/\Lambda)$, respectively, with a cutoff Λ . Note that a real solution y exists only when $T_{c,o} \leq T_{c,e}$. This implies that $\Omega_{\text{BS}} = 0$ indicates a transition between two superconducting states, and, in turn, Ω_{BS} can be understood to tell how much more the superconducting condensate is stable than other superconducting states.

We now use Eq. (18) to estimate Ω_{BS} in CeRh₂As₂ at zero field. Adopting $T_{c,o}/T_{c,e} = 0.87$ as estimated for CeRh₂As₂ by ref. 13, we find $\Omega_{\text{BS}} \sim 0.51\Delta_e$; i.e. below the pair-breaking continuum. It should be stressed that this estimation of Ω_{BS} from Eq. (18) has nothing to do with our choice of the parameters such as t, μ, α_R ; it is a model-independent result under weak-coupling assumption.

In Fig. 3b, the spectral functions $\text{Im}[1/[\tilde{\Pi}^{(o)}(\Omega)]_{22}]$ are drawn for several g_o/g_e around the critical ratio. The location of the peak of each curve corresponds to Ω_{BS} for each ratio g_o/g_e . The height of peak is enhanced as $g_o/g_e \rightarrow r_c$. The inset clearly shows that the peak height is inversely proportional to Ω_{BS} for small Ω_{BS} .

This is a general consequence resulted from $\tilde{\Pi}^{(o)}(\Omega) = [\tilde{\Pi}^{(o)}(\Omega)]^\dagger = [\tilde{\Pi}^{(o)}(-\Omega)]^{\text{T}45}$ for Ω below the quasiparticle continuum, which ensures $\det \tilde{\Pi}^{(o)}(\Omega) \propto \Omega_{\text{BS}}^2 - \Omega^2$ when Ω_{BS} and Ω are small. Given that the off-diagonal elements of $\tilde{\Pi}^{(o)}$ are small, then $\det \tilde{\Pi}^{(o)}(\Omega)$ and $[\tilde{\Pi}^{(o)}(\Omega)]_{22}$ are proportional, and we know $\text{Im}[1/[\tilde{\Pi}^{(o)}(\Omega)]_{22}] \propto \delta(\Omega_{\text{BS}}^2 - \Omega^2) \propto \delta(\Omega_{\text{BS}} - \Omega)/\Omega_{\text{BS}}$. Thus, the intensity of the BS mode increases as Ω_{BS} approaches to zero. Note that this argument is applicable even when magnetic fields are applied and also applicable to the BS mode in the oSC state except that the BS mode appears only when $g_o > g_{o,c}$.

Bardasis-Schrieffer mode under B_z . We now study the effect of magnetic fields on the BS mode. Figure 4a and b show the imaginary part of the inverse of $[\tilde{\Pi}^{(p)}(B_z, \Omega)]_{22}$ in the pSC state for B_z . Here, $g_o = 1.17g_e$ is used to make the features of figures more recognizable. The reddish region of each figure represents the BdG quasiparticle excitations. Below the quasiparticle continuum, the curves corresponding to the gap of the BS mode $\Omega_{\text{BS}}(B_z)$ in each pSC appear. The red and blue lines are drawn over the curves for a guide to the eye. The vertical dashed lines in both figures denote the even-to-odd critical field $B_{z,c}$ identified in Fig. 2a.

It is clearly seen that $\Omega_{\text{BS}}(B_z)$ in eSC (oSC) phase is lowered (raised) as the external magnetic field B_z increases. Also, it has to be noted that Ω_{BS} exhibits a jump at the transition as shown in Fig. 4c, which is generally expected for a first-order transition^{46–48}. Furthermore, Ω_{BS} becomes zero at $B_z = B_{z,e} > B_{z,c}$ ($B_z = B_{z,o} < B_{z,c}$) in eSC (oSC) phase. Recalling that the eSC (oSC) phase is the equilibrium ground state under $B_z < B_{z,c}$ ($B_z > B_{z,c}$), Figure 4 shows that the softening of the BS mode occurs outside the thermodynamic equilibrium^{31,49}. Understood as a precursor of an instability of a superconducting condensate, $B_{z,e}$ ($B_{z,o}$) could correspond to the termination of the metastability of the eSC (oSC) state. Note that this limiting field $B_{z,e}$ ($B_{z,o}$) is to the transition into the oSC (eSC) state what the superheating field is to the vanishing of the energy barrier against the vortex formation in type-II superconductors.

Multiband-assisted optical coupling. The linear optical response function of the BS mode can be given as

$$\tilde{K} = K - L^{(p)}[\tilde{\Pi}^{(p)}]^{-1}[L^{(p)}]^\dagger, \quad (19)$$

which is derived from $\mathcal{J}_i(i\Omega)/|e| = \delta S_{\text{eff}}^{(p)}/\delta A_i(-i\Omega) = K_{ij}(i\Omega)A_j(i\Omega) + L_{ia}^{(p)}(i\Omega)\eta_a(i\Omega)$, $R^{(p)}(i\Omega) = [L^{(p)}(-i\Omega)]^\dagger$ and Eq. (16) as exposed in the subsection "Derivation of \tilde{K} " in the "Methods" section. The imaginary part of $\tilde{K}(\Omega) \equiv \tilde{K}(i\Omega)|_{i\Omega \rightarrow \Omega^+}$ is related to the real part of the optical conductivity tensor $\sigma(\Omega) = \sigma_1(\Omega) - i\sigma_2(\Omega)$ by $\sigma_1(\Omega) = \text{Im}[\tilde{K}(\Omega)]/\Omega$. Note that $\sigma_1(\Omega)$ involves the contribution of the BS mode contained in the second term in the RHS of Eq. (19), and the contribution is finite only when $L_{i,a}^{(p)}(\Omega)$ is finite. This is often overlooked in literature partially due to the fact that the matrix elements of the velocity operators vanish in the BCS model with a single electronic band⁵⁰.

However, the presence of multiple electronic bands can render $L_{i,a}^{(p)}(\Omega)$ finite⁵¹, as explained in detail below based on the analytical estimation of it in the eSC state at zero field.

Since the symmetry group of $H_{\text{BdG}}^{(e)}$ makes $L_{x,2}^{(o)}$ and $L_{y,2}^{(o)}$ vanish as shown in the subsection "Other odd-parity pairing channels" in the "Methods" section, we focus on $L_{z,2}^{(o)}$. The spectral representation of it is given as $L_{z,2}^{(o)}(\Omega) = -\int \mathcal{L}(\mathbf{k}, \Omega) d^d \mathbf{k} / (2\pi)^d$ with

$$\mathcal{L}(\mathbf{k}, \Omega) = -\frac{1}{2} \sum_{m,n} \frac{\langle m | \mathcal{V}_z | n \rangle \langle n | \tau_y \sigma_z | m \rangle}{\Omega^+ - E_m + E_n} \Theta_{mn}, \quad (20)$$

at the zero-temperature, where $\Theta_{mn} \equiv \Theta(E_m) - \Theta(E_n)$ with the Heaviside step function $\Theta(x)$. E_m and $|m\rangle$ denote the eigenenergies $E_{c,i} = -E_{v,i} = \sqrt{\xi_i^2 + \Delta_c^2}$ and the corresponding eigenvectors $|c(v), i, u\rangle$ of the BdG Hamiltonian $H_{\text{BdG}}^{(e)}$, respectively, which are given in the subsection "Microscopic model" in the "Methods" section. The momentum dependence of E_m and $|m\rangle$ is omitted for conciseness.

The matrix element $\langle m | \mathcal{V}_z | n \rangle$ of the velocity operator, defined in the subsection "Macroscopic model" in the "Methods" section, relevant for calculating $L_{z,2}^{(o)}$ at the zero-temperature is given by

$$\langle c, i, u | \mathcal{V}_z | v, j, v \rangle = \sin \frac{\Xi_i - \Xi_j}{2} \langle i, u | \partial_z H_0 | j, v \rangle, \quad (21)$$

where $\sin \Xi_i \equiv \Delta_c / E_{c,i}$. Note that the RHS is zero when $i = j$, as it is in the single-band model. These forbidden elements $\langle c, i, u | \mathcal{V}_z | v, i, v \rangle$ for $u, v = \pm$ are marked by gray arrows in Fig. 5a, where the energy bands of the BdG quasiparticles are drawn. An explicit calculation using the eigenvectors $|i, u\rangle$ given in the subsection "Microscopic model" in the "Methods" section yields $\langle i, u | \partial_z H_0 | j, v \rangle \propto \delta_{uv}$. Therefore, only $\langle c, i, u | \mathcal{V}_z | v, j, u \rangle$ with $i \neq j$ for $i = 1, 2$ and their complex conjugate are finite. The colored arrows in Fig. 5a represent the transitions related to these finite elements of the velocity operator. Comparing these to the interband transitions in the normal phase whose electronic band structure is displayed in Fig. 5b, these finite transitions associated with $\langle m | \mathcal{V}_z | n \rangle$ can be understood as the remnants of the interband transitions in the normal phase which are marked by arrows in Fig. 5b⁵¹.

With $\langle c, j, u | \tau_y \sigma_z | v, i, u \rangle$ and their complex conjugate, one of which is given by

$$\langle c, 2, u | \tau_y \sigma_z | v, 1, u \rangle = \frac{e^{i(\zeta+\phi)} t_k \cos \chi}{2i} \cos \frac{\Xi_2 - \Xi_1}{2}, \quad (22)$$

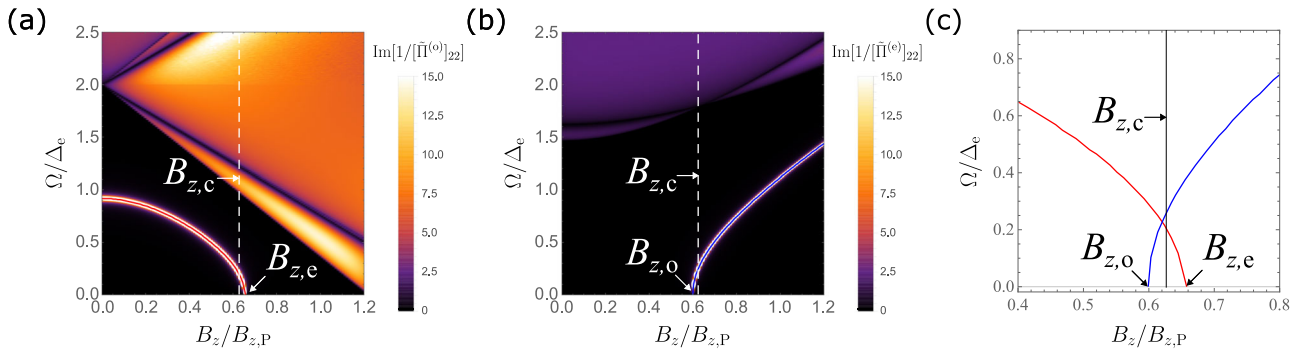


Fig. 4 Spectral function of the Bardasis-Schrieffer (BS) mode for $g_0 = 1.17g_e$ in the plane of frequency and magnetic field B_z . **a** False color plot of the spectral function $\text{Im}[1/[\tilde{\Pi}^{(e)}]_{22}]$ of the BS mode in the even-parity superconducting state. **b** False color plot of the spectral function $\text{Im}[1/[\tilde{\Pi}^{(o)}]_{22}]$ of the BS mode in the odd-parity superconducting state. $\Delta_o = 0.001$ is used which is obtained from Eq. (9) with $g_0 = 1.17g_e$. **c** The gaps of the BS modes. The red and blue lines are the lines of the same colors depicted in (a) and (b), respectively. The crossing point of the two curves does not coincide with the magnetic field $B_{z,c}$ at the first-order transition. Δ_e is the magnitude of the superconducting gap function in the even-parity superconducting state. $B_{z,p}$ is the Pauli limiting field. $B_{z,e}$ and $B_{z,o}$ are the magnetic fields at which the BS mode in each superconducting state becomes gapless.

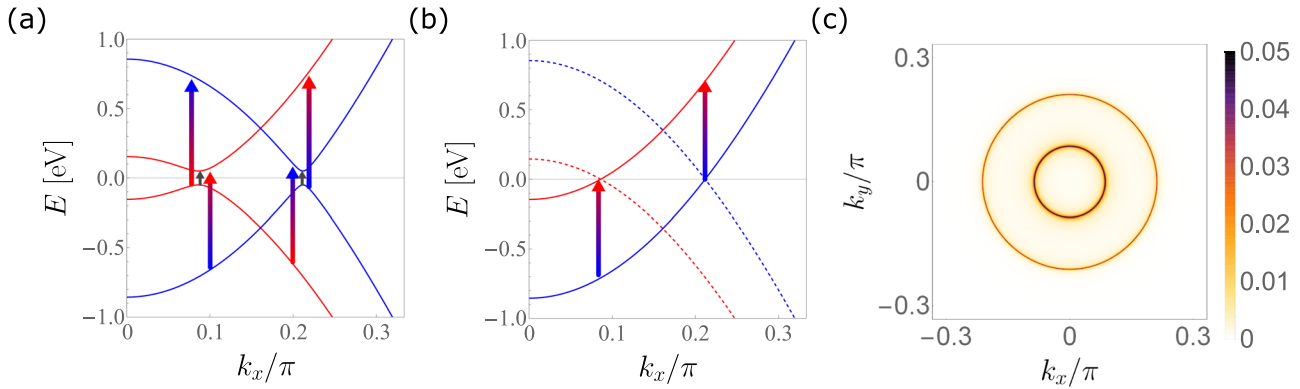


Fig. 5 The band structure and the transitions between bands contributing to $\mathcal{L}(\mathbf{k}, \Omega)$ in Eq. (20). **a** The band structure of the Bogoliubov-de Gennes quasiparticle and the transition relevant to $\mathcal{L}(\mathbf{k}, \Omega)$. The colored arrows depict the transitions contributing to $\mathcal{L}(\mathbf{k}, \Omega)$ in the even-parity superconducting state, while the gray arrows denote transitions to which have no contribution to $\mathcal{L}(\mathbf{k}, \Omega)$. **b** The electronic band structure is in the normal state. The interband transitions depicted by the colored arrows in (a) are inherited from the transitions depicted by the colored arrows in (b). For (a) and (b), the superconducting gap magnitude $\Delta_e = 0.05$ is used. **c** $\mathcal{L}(\mathbf{k}, 0)$ in the k_x - k_y plane. $\Delta_e = 0.004$ is used for (c).

we get

$$\mathcal{L}(\mathbf{k}, \Omega) = \frac{(E_{c,1} + E_{c,2})t(\mathbf{k}) \cos \chi \sin(\Xi_2 - \Xi_1)}{(E_{c,1} + E_{c,2})^2 - (\Omega^+)^2}. \quad (23)$$

Note that the possible singularities of $\mathcal{L}(\mathbf{k}, \Omega)$ are located at $|\Omega| = \Delta_e + |\xi_{1,\mathbf{k}} - \xi_{2,\mathbf{k}}|$ which are fairly distant from the region of interest $|\Omega| < 2\Delta_e$. Hence, it is a good approximation to set $\Omega = 0$ in Eq. (23). We draw $\mathcal{L}(\mathbf{k}, 0)$ in Fig. 5c. $\mathcal{L}(\mathbf{k}, 0)$ has narrow positive peaks of height $\frac{\Delta_e \cos^2 \chi}{4E_i(\mathbf{k})}$ on each i th Fermi surface, and thus

$$L_{z,2}^{(o)}(\Omega) \approx -\frac{\Delta_e \langle \cos^2 \chi \rangle_{\text{FS}}}{2g_e}. \quad (24)$$

Here, we use the BCS gap equation $1/g_e = (N_1 + N_2) \int d\xi (\xi^2 + \Delta_e^2)^{-1/2}$ with N_i the density of states of the i th Fermi surface given by $\xi_i = 0$. Note that $L_{z,2}^{(o)}(\Omega)$ is finite even at $\Omega = 0$ as long as $\langle \cos^2 \chi \rangle_{\text{FS}} \neq 0$, which is approximately proportional to t_c^2/α_R^2 . Thus, the signature of the BS mode is expected to be observed in the optical conductivity along the z -direction $[\sigma_1(\Omega)]_{zz}$, or just $\sigma_1(\Omega)$ for short, at zero field.

Optical response. Given that the coupling between the fluctuations in the uncondensed channel and the light can be finite, the signature of the BS mode can be observed by measuring the

optical conductivity $\sigma_1(\Omega)$. However, considering the experimental conditions by which the available range of frequency of the incident light is restricted, it is necessary to adjust the gap of the BS mode by tuning the external parameter, i.e. the magnetic field. Therefore, we present here our numerical results of $\sigma_1(\Omega)$ under B_z to provide a guide to future experiments.

For illustration, we use the case with $g_0 = 1.17g_e$ again. Figure 6a and b show $\sigma_1(B_z, \Omega)$ (normalized by $\sigma_1(0, 2.5\Delta_e)$) in the log-scale in the eSC and the oSC states, respectively. It is easy to see the signature from the collective modes appearing in the spectral function of the BS mode $\text{Im}[1/[\tilde{\Pi}_{22}^{(p)}(B_z, \Omega)]]$ in Fig. 4a and b. As illustrated in Fig. 4c, the gap of BS mode is expected to change discontinuously when the first-order transition occurs, and thus, a sudden jump of the peak due to the BS mode can be observed in σ_1 .

Since $L_{z,2}^{(p)}(B_z, \Omega)$ is finite in the range of interest, the collective mode makes distinguished contributions to $\sigma_1(B_z, \Omega)$ which increases as $\Omega_{\text{BS}} \rightarrow 0$ like $\text{Im}[1/[\tilde{\Pi}^{(o)}(\Omega)]_{22}]$ displayed in Fig. 3b. Figure 6c shows graphs of $\sigma_1(B_z, \Omega)$ for several B_z marked by stars in Fig. 6a, and we see that the peak height of $\sigma_1(B_z, \Omega)$ from the BS mode diverges like Ω_{BS}^{-2} around the point where the gap of the BS mode vanishes and the metastability of the eSC state is terminated, which is in sharp contrast to the case in the iron-based superconductors where the spectral weight of BS mode in Raman measurement is predicted to diminish as the softening is approached⁵²⁻⁵⁴. The diverging trend appears

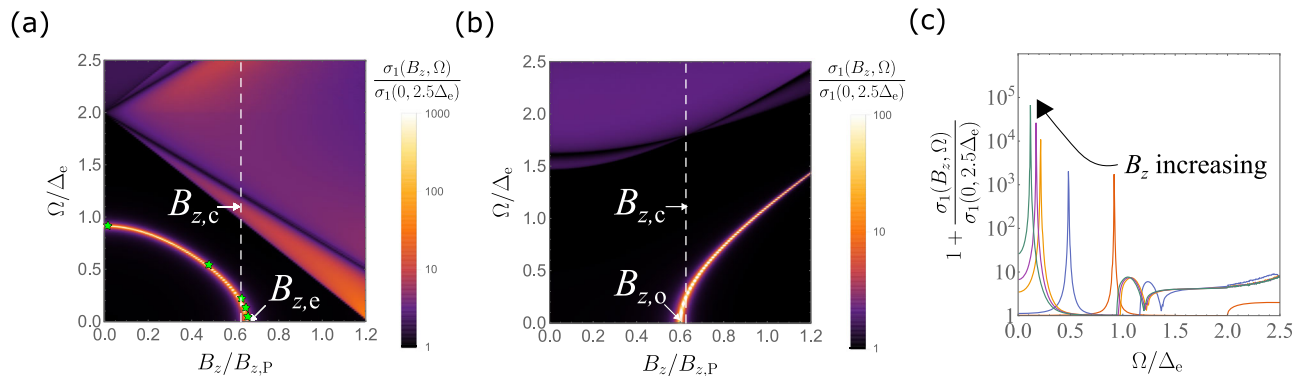


Fig. 6 The frequency and the magnetic field dependence of the real part of the optical conductivity $\sigma = \sigma_1 + i\sigma_2$. **a** False color plot of σ_1 in the even-parity superconducting state. **b** False color plot of σ_1 in the odd-parity superconducting state. $\Delta_e = 0.001$ is used which is obtained from Eq. (9) with $g_0 = 1.17g_e$. **c** Frequency dependence of σ_1 for several magnetic fields B_z marked by green stars in (a). σ_1 is normalized by its magnitude at zero field and $\Omega = 2.5\Delta_e$. For **c**, the unity is added to plot σ_1 on the semi-log scale. $B_{z,c}$ and $B_{z,p}$ are the magnetic fields at the first-order transition and the Pauli limiting field, respectively. $B_{z,e}$ and $B_{z,o}$ are the magnetic fields at which the Bardasis-Schrieffer mode in each superconducting state becomes gapless.

because $I_{z,a}^{(p)}(B_z, \Omega)$ is almost constant up to the critical magnetic field $B_{z,e}$ ($B_{z,o}$) where the BS mode in the eSC (oSC) state becomes gapless. Consequently, using an incident light of lower frequency, a stronger peak from the BS mode is expected. The trend of $\sigma_1(B_z, \Omega)$ in the oSC state is qualitatively identical except that the peak height of the BS mode increases with decreasing B_z .

Discussion

We have investigated the linear optical response from the BS modes brought about by the uncondensed pairing channel with parity opposite to that of the condensed pairing. Our analysis shows the gap of the BS mode in the eSC (oSC) state is lowered with the increasing (decreasing) out-of-plane magnetic field and eventually becomes gapless at the termination of the metastability of the superconducting condensate which occurs around the first-order transition. In our analysis, the presence of the multiple orbital degrees of freedom intertwined by the inversion symmetry turns out to be crucial as it enables the linear coupling between the BS mode and the light which is generally allowed by the symmetry. As long as this coupling is finite, the contribution to the optical conductivity of the BS mode is much larger than that of the quasiparticle excitation in the clean limit and also can get enhanced as the BS mode softens. Therefore, we can expect the signature of the collective mode to be observed by measuring the linear optical response in the microwave regime for the superconductor CeRh_2As_2 , where $\Omega_{\text{BS}} \sim 0.51\Delta_e$ is expected at zero field^{55–58}.

It should be stressed that the detection of the BS modes via a linear optical response measurement is a compelling signature from the bulk of CeRh_2As_2 evidencing the competing odd-parity pairing channel. This is because linear optical coupling is possible only when the condensed and the competing uncondensed pairing channels are opposite in parity. Moreover, as discussed in the subsection “Other odd-parity channels” in the “Methods” section, the light selectively couples to a particular set of odd-parity pairings transforming as A_{2u} for D_{4h} symmetry to which the current operator along z belongs. Therefore, the detection of the BS modes not only can be taken as compelling proof, i.e. sufficient, for the existence of the odd-parity pairing channel but also can place restrictions on the form of the odd-parity pairing channels³¹. It also deserves to be noted that the gap of the BS mode in the oSC increases with increasing

out-of-plane magnetic field. This feature may also be regarded as proof of the parity-switching at the first-order transition in the superconducting phase of CeRh_2As_2 because the gap of the BS mode should continue decreasing if it were not for the parity-switching.

Though the Pauli paramagnetic depairing is considered the primary cause of the first-order transition in the superconducting state of CeRh_2As_2 , our findings and argument are applicable to any superconducting systems exhibiting parity-switching transitions regardless of the underlying mechanism and the transition order. An interesting application is superconductivity in a system hosting a structural instability^{9,11,12,59}, e.g. ferroelectric instability. We address the cases from the two perspectives. Firstly, if the even-to-odd transition is realized within the centrosymmetric state of this system, it is possible to have a soft BS mode at the transition, and a signature from it can appear in the linear optical response.

The second case is when such a transition occurs in the non-centrosymmetric state. In this case, the superconducting phase could host an intriguing topological phase transition between an even-parity dominant trivial superconductivity and an odd-parity dominant topological superconductivity, and a low-lying Leggett mode could appear at the transition^{11,12}. The existence of such a topological phase transition implies there are at least two competing pairing channels of opposite parities up to the parity mixing induced by the inversion-breaking order. This parity mixing blurs the sharp distinction between even- and odd-parity pairings, which could lead both pairing channels to belonging to the same irreducible representation of the symmetry group of the state. As a result, the BS mode from the competing pairing channel will turn into the Leggett mode of refs. ^{11,12}. The absence of the inversion symmetry could allow the linear optical coupling of this Leggett mode to be nonzero⁵¹.

Lastly, a recent experiment suggests that the possibility of an inversion-breaking antiferromagnetic order coexisting with superconductivity in CeRh_2As_2 ^{42,60}. Since the antiferromagnetic order can reduce the symmetry group of the system, its potential effect on the BS modes and the optical response calls for further investigation.

Note added in proof: During the revision of this work for publication, ref. ⁶¹ appeared in arxiv. This work investigates the BS mode arising from the odd-parity pairing in a two-dimensional bilayer system and the consequence of the presence of strong interlayer Coulomb interaction.

Methods

Microscopic model. The two-fold degenerate eigenenergies of $H_0(\mathbf{k})$ in Eq. (1) are given by

$$\xi_1(\mathbf{k}) = \varepsilon_{00}(\mathbf{k}) - \mu + \sqrt{t(\mathbf{k})^2 + \alpha(\mathbf{k})^2}, \quad (25)$$

$$\xi_2(\mathbf{k}) = \varepsilon_{00}(\mathbf{k}) - \mu - \sqrt{t(\mathbf{k})^2 + \alpha(\mathbf{k})^2}, \quad (26)$$

with $t(\mathbf{k}) = \sqrt{\varepsilon_{10}(\mathbf{k})^2 + \varepsilon_{20}(\mathbf{k})^2}$ and $\alpha(\mathbf{k}) = \sqrt{\varepsilon_{31}(\mathbf{k})^2 + \varepsilon_{32}(\mathbf{k})^2}$. The eigenvectors of these eigenvalues are

$$|\xi_1, +\rangle = \begin{pmatrix} \frac{\cos \frac{\chi}{2}}{\sqrt{2}} \\ \frac{e^{i\phi} \sin \frac{\chi}{2}}{\sqrt{2}} \\ \frac{e^{i\chi} \cos \frac{\chi}{2}}{\sqrt{2}} \\ z \frac{\sin \frac{\chi}{2}}{-\sqrt{2}} \end{pmatrix}, \quad |\xi_1, -\rangle = \begin{pmatrix} \frac{\sin \frac{\chi}{2}}{z\sqrt{2}} \\ \frac{e^{-i\chi} \cos \frac{\chi}{2}}{\sqrt{2}} \\ \frac{e^{-i\phi} \sin \frac{\chi}{2}}{-\sqrt{2}} \\ \frac{\cos \frac{\chi}{2}}{\sqrt{2}} \end{pmatrix}, \quad (27a)$$

$$|\xi_2, +\rangle = \begin{pmatrix} \frac{\cos \frac{\chi}{2}}{z\sqrt{2}} \\ \frac{e^{-i\chi} \sin \frac{\chi}{2}}{-\sqrt{2}} \\ \frac{e^{-i\phi} \cos \frac{\chi}{2}}{-\sqrt{2}} \\ \frac{\sin \frac{\chi}{2}}{-\sqrt{2}} \end{pmatrix}, \quad |\xi_2, -\rangle = \begin{pmatrix} \frac{\sin \frac{\chi}{2}}{\sqrt{2}} \\ \frac{e^{i\phi} \cos \frac{\chi}{2}}{-\sqrt{2}} \\ \frac{e^{i\chi} \sin \frac{\chi}{2}}{\sqrt{2}} \\ \frac{z \cos \frac{\chi}{2}}{\sqrt{2}} \end{pmatrix}, \quad (27b)$$

with $\exp(i\chi) = \{t(\mathbf{k}) + i\alpha(\mathbf{k})\} / \sqrt{t(\mathbf{k})^2 + \alpha(\mathbf{k})^2}$, $\exp(i\zeta) = \{\varepsilon_{10}(\mathbf{k}) + i\varepsilon_{20}(\mathbf{k})\} / t(\mathbf{k})$, $\exp(i\phi) = \{\varepsilon_{31}(\mathbf{k}) + i\varepsilon_{32}(\mathbf{k})\} / \alpha(\mathbf{k})$, and $z = \exp[i(\zeta + \phi)]$.

The eigenenergies and eigenvectors of $H_{\text{BdG}}^{(e)}$ at zero field are given by $E_{c,i} = -E_{v,i} = \sqrt{\xi_i^2 + \Delta_e^2}$ for $i = 1, 2$ and

$$|c, i, u\rangle = \begin{pmatrix} \cos \frac{\Xi_i}{2} |\xi_i, u\rangle \\ \sin \frac{\Xi_i}{2} |\xi_i, u\rangle \end{pmatrix}, \quad (28)$$

$$|v, i, u\rangle = \begin{pmatrix} -\sin \frac{\Xi_i}{2} |\xi_i, u\rangle \\ \cos \frac{\Xi_i}{2} |\xi_i, u\rangle \end{pmatrix},$$

for $u = \pm$ with $e^{i\Xi_i} = (\xi_i + i\Delta_e) / E_{c,i}$. These are used in the main text to derive the approximate expression for $L_{z,2}^{(e)}(\Omega)$.

Macroscopic model. By adding

$$\hat{V} = -\frac{1}{2} \sum_p \sum_{k_1, k_2, q} g_p \hat{\Pi}_p(k_1, k_1 - q) [\hat{\Pi}_p(k_2, k_2 - q)]^\dagger \quad (29)$$

to the normal phase action $\mathcal{S}_0 = \frac{1}{2} \sum_k \hat{\Psi}_k^\dagger (i\omega - H_0) \hat{\Psi}_k$, and using the Hubbard–Stratonovich transformation, the microscopic action including the pairing fluctuations is obtained:

$$\mathcal{S} = \mathcal{S}_e^{(p)} + \mathcal{S}_{e-\eta} + \mathcal{S}_\eta + \mathcal{S}_{e-A}, \quad (30)$$

$$\mathcal{S}_e^{(p)} = \frac{1}{2} \sum_k \hat{\Psi}^\dagger(k) \{-i\omega + H_{\text{BdG}}^{(p)}(\mathbf{k})\} \hat{\Psi}(k), \quad (31)$$

$$\mathcal{S}_\eta = \frac{1}{2} \sum_{p,a} \sum_q \frac{\hat{\eta}_a^{(p)}(q) \hat{\eta}_a^{(p)}(-q)}{g_p}, \quad (32)$$

$$\mathcal{S}_{e-\eta} = \frac{1}{2} \sum_{p,a,k,q} \hat{\Psi}^\dagger(k+q) \{\eta_a^{(p)}(q) \tau_a^{(p)}\} \hat{\Psi}(k), \quad (33)$$

$$\mathcal{S}_{e-A} = \frac{1}{2} \sum_{k,q} \hat{\Psi}^\dagger(k+q) \{\Gamma_1(\mathbf{k}, q) + \Gamma_2(k, q)\} \hat{\Psi}(k). \quad (34)$$

The auxiliary bosonic fields $\eta_1^{(p)}$ and $\eta_2^{(p)}$ represent the real and imaginary parts of the fluctuation in the condensed pairing channel of the pSC state, respectively. Γ_1 and Γ_2 are the

paramagnetic and diamagnetic light-matter coupling vertices, respectively, and expressed in the uniform limit ($\mathbf{q} \rightarrow 0$) of the external electromagnetic fields as

$$\Gamma_1(\mathbf{k}, q) = \sum_{\mu=0}^3 \mathcal{V}_\mu(\mathbf{k}) \mathcal{A}_\mu(q), \quad (35)$$

$$\Gamma_2(k, q) = \sum_{k'} \sum_{\mu, \nu=0}^3 [m_k^{-1}]_{\mu\nu} \mathcal{A}_\mu(q - k') \mathcal{A}_\nu(k'), \quad (36)$$

with the four-velocity operators $\mathcal{V}_\mu(\mathbf{k}) = (2\tau_z, \tau_0 \partial_i H_0(\mathbf{k}))$ and the inverse of the mass matrix $[m_k^{-1}]_{\mu\nu} = \tau_z \partial_\mu \partial_\nu H_0(\mathbf{k})$ which is zero when either of μ or ν is 0. Here, we define a four-potential $\mathcal{A}_\mu = |e|(-iA_0, \mathbf{A})$ by multiplying the unit charge $|e|$ to the conventional four-potential for conciseness.

By integrating out the fermionic degree of freedom $\hat{\Psi}$ and expanding the resultant action to the second order in \mathcal{A}_μ and $\eta_a^{(p)}$, we obtain an effective action for η and \mathcal{A} :

$$\mathcal{S}_{\text{eff}}^{(p)} = \frac{1}{2} \sum_{\Omega} (\mathcal{A}_0, \eta_a^{(p)})_{-i\Omega} \begin{pmatrix} K_{00} & L_{0b}^{(p)} \\ R_{0\nu}^{(p)} & \tilde{\Pi}_{ab}^{(p)} \end{pmatrix} \begin{pmatrix} \mathcal{A}_0 \\ \eta_b^{(p)} \end{pmatrix}_{i\Omega} \quad (37)$$

$$+ \frac{1}{2} \sum_{\Omega} (\mathcal{A}_i, \eta_a^{(p)})_{-i\Omega} \begin{pmatrix} K_{ij} & L_{ib}^{(p)} \\ R_{aj}^{(p)} & \tilde{\Pi}_{ab}^{(p)} \end{pmatrix} \begin{pmatrix} \mathcal{A}_j \\ \eta_b^{(p)} \end{pmatrix}_{i\Omega},$$

where \bar{p} denotes the odd-parity(even-parity) pairing channel in eSC (oSC) state, which is the uncondensed pairing channel. Note that we omit the momentum \mathbf{q} dependence of η and \mathcal{A} since the London limit ($\mathbf{q} \rightarrow 0$) of the linear response is our interest. The sub-blocks K , L , R , and $\tilde{\Pi}$ are given by

$$K_{\mu\nu}(q) = \frac{1}{2} \sum_k \text{Tr} [\mathcal{V}_\mu(\mathbf{k}) G(k+q) \mathcal{V}_\nu(\mathbf{k}) G(k)] + \sum_k \text{Tr} [G(k) [m_k^{-1}]_{\mu\nu}], \quad (38)$$

$$L_{\mu a}^{(p)}(q) = \frac{1}{2} \sum_k \text{Tr} [\mathcal{V}_\mu(\mathbf{k}) G(k+q) \tau_a^{(p)} G(k)], \quad (39)$$

$$R_{a\mu}^{(p)}(q) = \frac{1}{2} \sum_k \text{Tr} [\tau_a^{(p)} G(k+q) \mathcal{V}_\mu(\mathbf{k}) G(k)], \quad (40)$$

$$\tilde{\Pi}_{ab}^{(p)}(q) = \frac{\delta_{ab}}{g_p} + \frac{1}{2} \sum_k \text{Tr} [\tau_a^{(p)} G(k+q) \tau_b^{(p)} G(k)], \quad (41)$$

with $q = (i\Omega, \mathbf{0})$ and for $p = e, o$.

Derivation of \tilde{K} . The current $J_i(\Omega)$ in response to the external electromagnetic vector potential is derived by differentiating $\mathcal{S}_{\text{eff}}^{(p)}$ with respect to the vector potential $\mathcal{A}_i(-i\Omega)$ and then taking the analytic continuation $i\Omega \rightarrow \Omega + ie$.

$$J_i(\Omega) = \left. \frac{\delta \mathcal{S}_{\text{eff}}^{(p)}}{\delta \mathcal{A}_i(-i\Omega)} \right|_{i\Omega \rightarrow \Omega + ie} \quad (42)$$

$$= K_{ij}(\Omega) \mathcal{A}_j(\Omega) + L_{ia}^{(p)}(\Omega) \eta_a^{(p)}(\Omega),$$

where we use an identity $K_{ij}(\Omega) = K_{ji}(-\Omega)$ and $L_{ia}^{(p)}(\Omega) = R_{ai}^{(p)}(-\Omega)$. By substituting $\eta^{(p)} = -[\tilde{\Pi}^{(p)}]^{-1} R^{(p)} \mathcal{A}$ for $\eta^{(p)}$ in Eq. (42), we obtain

$$J_i = \left\{ K_{ij} - [L^{(p)} [\tilde{\Pi}^{(p)}]^{-1} R^{(p)}]_{ij} \right\} \mathcal{A}_j, \quad (43)$$

where the argument Ω of each function is omitted for conciseness. Note that the term in parenthesis is nothing but \tilde{K} in Eq. (19).

Spectral representation of $L_{z,2}^{(0)}$ in the eSC state. The spectral representation of $L_{\mu a}^{(p)}(q)$ is derived by carrying out the Matsubara frequency summation. Starting with the definition, we obtain

$$\begin{aligned} L_{\mu a}^{(p)}(\Omega) &= \frac{1}{2} \sum_k \text{Tr} [\mathcal{V}_{\mu, k} G(i\omega_n + i\Omega_\nu, \mathbf{k}) \tau_a^{(p)} G(\mathbf{k})] \Big|_{i\Omega_\nu \rightarrow \Omega^+} \\ &= \frac{1}{2} \sum_k \frac{\langle m, \mathbf{k} | \mathcal{V}_{\mu, k} | n, \mathbf{k} \rangle \langle n, \mathbf{k} | \tau_a^{(p)} | m, \mathbf{k} \rangle}{(i\omega_u + i\Omega_\nu - E_{n, \mathbf{k}})(i\omega_u - E_{m, \mathbf{k}})} \Big|_{i\Omega_\nu \rightarrow \Omega^+} \\ &= \frac{1}{2} \sum_k \frac{\langle m, \mathbf{k} | \mathcal{V}_{\mu, k} | n, \mathbf{k} \rangle \langle n, \mathbf{k} | \tau_a^{(p)} | m, \mathbf{k} \rangle}{\Omega^+ - E_{n, \mathbf{k}} + E_{m, \mathbf{k}}} \Theta_{mn, \mathbf{k}}, \end{aligned} \quad (44)$$

where $\Theta_{mn, \mathbf{k}} \equiv \Theta(E_{m, \mathbf{k}}) - \Theta(E_{n, \mathbf{k}})$ and $\Omega^+ = \Omega + i\epsilon$.

Other odd-parity channels. In this section, we discuss the linear couplings between the other odd-parity channels and the light (or the current) when the zero-field ground state is an even-parity state. We first note that the presence of an inversion $\mathcal{I} = \sigma_x$ and a time-reversal symmetry $\mathcal{T} = i s_y \mathcal{K}$ forces the normal phase Hamiltonian to take the following form:

$$H_0(\mathbf{k}) = \varepsilon_{00}(\mathbf{k})\sigma_0 s_0 + (\varepsilon_{10}(\mathbf{k})\sigma_x + \varepsilon_{20}(\mathbf{k})\sigma_y) s_0 + \sigma_z (\varepsilon_{31}(\mathbf{k})s_x + \varepsilon_{32}(\mathbf{k})s_y + \varepsilon_{33}(\mathbf{k})s_z) \quad (45)$$

where $\varepsilon_{00}(\mathbf{k})$ and $\varepsilon_{10}(\mathbf{k})$ are even functions under $\mathbf{k} \rightarrow -\mathbf{k}$ while $\varepsilon_{20}(\mathbf{k})$ and $\varepsilon_{3i}(\mathbf{k})$ are odd functions. The linear coupling between a pairing channel and the light is possible only when the pairing channel transforms like one of the current operators J_i under the symmetries of $H_0(\mathbf{k})$. For CeRh₂As₂, the point group D_{4h} is the symmetry of the Hamiltonian at Γ in the Brillouin zone. By using the symmetries of the point group D_{4h} , we analyze the selection rule for odd-parity channels transforming like $k_x s_y - k_y s_x$, $k_z s_z$, $k_z \sigma_x s_z$, or $k_x s_x + k_y s_y$ which are discussed in ref. 41.

Table 1 summarizes the parities of the current operators and the form factors of those odd-parity channels with respect to several two-fold symmetries in D_{4h} . The signs tell whether $TO(\mathbf{k})T^{-1} = +O(T\mathbf{k})$ or $TO(\mathbf{k})T^{-1} = -O(T\mathbf{k})$ where O represents one of the currents or the form factors in the first column of Table 1 and T represents a symmetry transformation in the first row.

Firstly, the linear coupling between the in-plane currents J_x and J_y and the odd-parity gap functions in Table 1 is forbidden by, for example, C_{2z} . It is easy to see that the odd-parity channels transforming like $k_x s_x + k_y s_y$ or $k_z s_z$ can not be linearly coupled to the light because of C_{2z} and C_{2x} . The odd-parity channel labeled by $k_x s_y - k_y s_x$ transforms like J_z for all two-fold symmetries in D_{4h} . Indeed, J_z and $k_x s_y - k_y s_x$ belong to the same irreducible representation, and thus $k_x s_y - k_y s_x$ can be coupled to the light as σ_z can.

	$\mathcal{I} (\sigma_x)$	$C_{2z} (s_z)$	$C_{2x} (\sigma_x s_x)$	$\mathcal{A} (\sigma_y s_x \mathcal{K})$
J_z, σ_z	–	+	–	–
$\{J_x, J_y\}$	–	–	$\{+, -\}$	–
$k_x s_y - k_y s_x$	–	+	–	+
$k_z s_z$	–	+	+	–
$k_x s_x + k_y s_y$	–	+	+	+
$k_z \sigma_x s_z$				

The first column shows the forms of the odd-parity gap functions considered as well as the current operators. The first row shows the representative two-fold symmetries of the normal state Hamiltonian H_0 in Eq. (45). \mathcal{A} is the antiunitary antisymmetry of $H_0(\mathbf{k})$ in Eq. (46). The matrix representations of the two-fold symmetries are given in the parentheses. The signs \pm mean $TO\mathbf{T}^{-1} = \pm O$ where O is an operator in the first column and T is a two-fold symmetry in the first row.

In the above symmetry-based analysis, however, the details of the electronic structure are not taken into consideration. For CeRh₂As₂, the large contribution to $\varepsilon_{33}(\mathbf{k})$ may be supposed to originate from the Ising-type spin-orbit couplings between next-nearest-neighboring Ce atoms. As long as this Ising-type spin-orbit coupling is so negligible that ε_{33} is also negligible compared to other ε_{ij} , the coupling between $k_x s_y - k_y s_x$ and J_z is expected to be much smaller than that between σ_z and J_z .

To prove it, we first note that the non-trivial part of the normal phase Hamiltonian

$$\tilde{H}_0(\mathbf{k}) \equiv H_0(\mathbf{k}) - \varepsilon_{00}(\mathbf{k})\sigma_0 s_0 \quad (46)$$

is subject to an additional antiunitary antisymmetry $\mathcal{A} = U_{\mathcal{A}} \mathcal{K}$ of $\tilde{H}_0(\mathbf{k})$ with $U_{\mathcal{A}} = i\sigma_y s_x$. It transforms under \mathcal{A} as $U_{\mathcal{A}} \tilde{H}_0(\mathbf{k})^* U_{\mathcal{A}}^\dagger = -\tilde{H}_0(\mathbf{k})$. By \mathcal{A} , the eigenvectors $|\xi_1, \alpha\rangle$ and $|\xi_1, \beta\rangle$ are related to $|\xi_2, \alpha\rangle$ and $|\xi_2, \beta\rangle$:

$$\mathcal{A}|\xi_1, \alpha\rangle = \sum_{\alpha'=\alpha, \beta} [\Gamma_{\mathcal{A}}]_{\alpha', \alpha} |\xi_2, \alpha'\rangle, \quad (47)$$

$$\mathcal{A}|\xi_2, \alpha\rangle = \sum_{\alpha'=\alpha, \beta} [-\Gamma_{\mathcal{A}}^T]_{\alpha', \alpha} |\xi_1, \alpha'\rangle, \quad (48)$$

where $\Gamma_{\mathcal{A}}$ is a 2×2 unitary matrix. Here, we use $U_{\mathcal{A}} = -U_{\mathcal{A}}^T$.

The antiunitary antisymmetry of \tilde{H}_0 is especially useful when the linear coupling is computed between the current operator J_z and the pairing fluctuations with the form factor $M_{\mathbf{k}}$ in the eSC state with the trivial ground state gap function. In the calculation, we frequently encounter terms such as $\mathcal{I}_{m\bar{m}} = \sum_{\alpha, \beta} \langle m, \alpha | J_z | \bar{m}, \beta \rangle \langle \bar{m}, \beta | M_{\mathbf{k}} | m, \alpha \rangle$ with $\bar{m} = -m$ being 1 or 2, which determine the selection rule for the optical response. A tedious manipulation leads us to

$$\mathcal{I}_{m\bar{m}} = \lambda_J \lambda_M \mathcal{I}_{m\bar{m}}, \quad (49)$$

where $\lambda_{\mathcal{O}}$ is the parity of the operator \mathcal{O} with respect to \mathcal{A} . Thus, if $\lambda_J \lambda_M = -1$, the linear coupling between the light and the pairing fluctuation characterized by the form factor $M_{\mathbf{k}}$ is forbidden. Note that both J_z and σ_z are odd under \mathcal{A} while $k_x s_y - k_y s_x$ is even. Therefore, the linear coupling between the light and the fluctuation in the pairing channel $k_x s_y - k_y s_x$ is negligible as long as the Ising-type spin-orbit coupling is negligible. This argument is also applicable even when the Zeeman term $B_z s_z$ induced by the out-of-plane magnetic field is added to $\tilde{H}_0(\mathbf{k})$.

For completeness, let us discuss the case discussed in ref. 21 in which it is proposed that the $H-T$ phase diagram of the superconducting states of CeRh₂As₂ might be reproduced with inter-layer spin-triplet odd-parity gap functions. There, the low-field state is characterized by an odd-parity spin-triplet gap function transforming like $k_x k_y k_z (k_x^2 - k_y^2) \sigma_x s_z$ that belongs to A_{1u} of D_{4h} . The gap function of the high-field state is another odd-parity spin-triplet gap function transforming $\sigma_y s_z$ belonging to A_{1u} of D_{4h} . For this case, a BS mode should exist because both pairing channels belong to different irreducible representations. Since both pairing channels have the same inversion parity, however, the BS mode is inactive in the linear optical response.

Relation between the critical temperatures and BS mode gap.

Eq. (17) is derived in this section. To derive it, it is sufficient to obtain the analytical expression of $\Pi_{22}^{(0)}(\Omega) = g_0^{-1} - \tilde{\Pi}_{22}^{(0)}(\Omega)$ for $|\Omega| < 2\Delta_e$. To get to the point first,

$$\Pi_{22}^{(0)}(\Omega) \approx -\langle \sin^2 \chi \rangle \left\{ \frac{1}{g_0} + N_{\text{tot}} \frac{2y \arcsin y}{\sqrt{1-y^2}} \right\}. \quad (50)$$

with $y = \Omega^+ / 2\Delta_e$ and $N_{\text{tot}} = N_1 + N_2$, which is used throughout this section. Here, N_i is the density of states at the Fermi surface

from the band ξ_i . (Counting the Kramer degeneracy, $2N_{\text{tot}}$ is the total density of states).

For later use, we first evaluate $\Pi_{22}^{(0)}$ using the identity

$$[\tau_z \sigma_z, G(k)^{-1}] = -2i\tau_y^{(0)} \text{Re}[\Delta_e] - 4iF_A. \quad (51)$$

where $4iF_A \equiv [\sigma_z, H_0]$. This commutator appears in literature that is concerned with the concept of superconducting fitness²¹. When the Ising-type spin-orbit coupling is ignored ($\lambda_1 = 0$) in Eq. (1), $F_A = J_z$ is satisfied. Given the self-consistent gap equation $2\text{Re}[\Delta_e] = -g_e \text{Tr}[\tau_x G(k)]$ and $F_A = J_z$, we get

$$\Pi_{22}^{(0)} = -\frac{1}{g_e} - \sum_k \frac{\text{Tr}[\tau_y \sigma_z G(k) F_A(\mathbf{k}) G(k)]}{\text{Re}[\Delta_e]} \quad (52)$$

$$= -\frac{1}{g_e} - \frac{2L_{z,2}^{(0)}(0)}{\text{Re}[\Delta_e]} \approx -\frac{\langle \sin^2 \chi \rangle}{g_e}, \quad (53)$$

where we use Eq. (24) for the last approximation.

To calculate $\Pi_{22}^{(0)}(\Omega)$, let us first decompose $\Pi_{22}^{(0)}(\Omega)$ at zero-temperature into the singular and regular parts as

$$\Pi_{22}^{(0)}(\Omega) = \Pi_{22}^{(0, \text{sig})}(\Omega) + \Pi_{22}^{(0, \text{reg})}(\Omega), \quad (54)$$

with

$$\Pi_{22}^{(0, \text{sig})}(\Omega) = \sum_k \sum_{i=1,2} \frac{4E_{c,i} \sin^2 \chi}{(\Omega^+)^2 - 4E_{c,i}^2}, \quad (55)$$

$$\Pi_{22}^{(0, \text{reg})}(\Omega) = \sum_k \frac{4\cos^2 \chi \cos^2 \frac{\Xi_1 - \Xi_2}{2} (E_{c,1} + E_{c,2})}{(\Omega^+)^2 - (E_{c,1} + E_{c,2})^2},$$

where we use

$$|\langle \xi_i, s | \sigma_z | \xi_j, s' \rangle| = (1 - \delta_{ss'}) \begin{cases} |\sin \chi| & i = j \\ |\cos \chi| & i \neq j \end{cases}, \quad (56)$$

$$\langle c, i, s | \tau_y^{(0)} | v, j, s' \rangle = \frac{1}{i} \cos \frac{\Xi_j - \Xi_i}{2} \langle \xi_i, s | \sigma_z | \xi_j, s' \rangle. \quad (57)$$

The potential singularities of $\Pi_{22}^{(0, \text{reg})}(\Omega)$ lie at $\Omega = E_{c,1} + E_{c,2} \gg 2\Delta_e$, and thus it behaves regularly for $|\Omega| < 2\Delta_e$. Also, it is expected to be very small compared to the singular part $\Pi_{22}^{(0, \text{sig})}$. Thus, ignoring it can be justified as far as the semi-analytical expression for Ω_{BS} is concerned. This approximation, $\Pi_{22}^{(0)}(\Omega) - \Pi_{22}^{(0)}(0)$ is given by

$$\begin{aligned} \Pi_{22}^{(0)}(\Omega) - \Pi_{22}^{(0)}(0) &= \sum_k \sum_i \frac{(\Omega^+)^2 \sin^2 \chi}{E_{c,i}((\Omega^+)^2 - 4E_{c,i}^2)} \\ &= -\langle \sin^2 \chi \rangle N_{\text{tot}} \frac{2y \arcsin y}{\sqrt{1-y^2}}. \end{aligned} \quad (58)$$

Therefore, we obtain

$$\begin{aligned} \tilde{\Pi}_{22}^{(0)}(\Omega) &= \frac{1}{g_0} + \Pi_{22}^{(0)}(\Omega) \\ &= \frac{1}{g_0} - \langle \sin^2 \chi \rangle \left(\frac{1}{g_e} + \frac{2N_{\text{tot}} y \arcsin y}{\sqrt{1-y^2}} \right). \end{aligned} \quad (59)$$

Data availability

The data that support the findings of this study are available from the corresponding authors upon reasonable request.

Code availability

All relevant code used in this study is available from the corresponding authors upon reasonable request.

Received: 9 March 2023; Accepted: 5 October 2023;

Published online: 20 October 2023

References

- Joynt, R. & Taillefer, L. The superconducting phases of UPt_3 . *Rev. Mod. Phys.* **74**, 235–294 (2002).
- Ishida, K. et al. Spin-triplet superconductivity in UNi_2Al_3 revealed by the ^{27}Al knight shift measurement. *Phys. Rev. Lett.* **89**, 037002 (2002).
- Mackenzie, A. P., Scaffidi, T., Hicks, C. W. & Maeno, Y. Even odder after twenty-three years: the superconducting order parameter puzzle of Sr_2RuO_4 . *npj Quantum Mater.* **2**, 40 (2017).
- Pustogow, A. et al. Constraints on the superconducting order parameter in Sr_2RuO_4 from oxygen-17 nuclear magnetic resonance. *Nature* **574**, 72–75 (2019).
- Ishida, K., Manago, M., Kinjo, K. & Maeno, Y. Reduction of the ^{17}O Knight shift in the superconducting state and the heat-up effect by NMR pulses on Sr_2RuO_4 . *J. Phys. Soc. Japan* **89**, 1–8 (2020).
- Petsch, A. N. et al. Reduction of the spin susceptibility in the superconducting state of Sr_2RuO_4 observed by polarized neutron scattering. *Phys. Rev. Lett.* **125**, 217004 (2020).
- Suh, H. G. et al. Stabilizing even-parity chiral superconductivity in Sr_2RuO_4 . *Phys. Rev. Res.* **2**, 032023 (2020).
- Käser, S. et al. Interorbital singlet pairing in Sr_2RuO_4 : a Hund's superconductor. *Phys. Rev. B* **105**, 155101 (2022).
- Kozii, V. & Fu, L. Odd-parity superconductivity in the vicinity of inversion symmetry breaking in spin-orbit-coupled systems. *Phys. Rev. Lett.* **115**, 207002 (2015).
- Schumann, T. et al. Possible signatures of mixed-parity superconductivity in doped polar SrTiO_3 films. *Phys. Rev. B* **101**, 100503 (2020).
- Wang, Y., Cho, G. Y., Hughes, T. L. & Fradkin, E. Topological superconducting phases from inversion symmetry breaking order in spin-orbit-coupled systems. *Phys. Rev. B* **93**, 1–13 (2016).
- Wang, Y. & Fu, L. Topological phase transitions in multicomponent superconductors. *Phys. Rev. Lett.* **119**, 187003 (2017).
- Khim, S. et al. Field-induced transition within the superconducting state of CeRh_2As_2 . *Science* **373**, 1012–1016 (2021).
- Hafner, D. et al. Possible quadrupole density wave in the superconducting Kondo lattice CeRh_2As_2 . *Phys. Rev. X* **12**, 011023 (2022).
- Maruyama, D., Sigrist, M. & Yanase, Y. Locally non-centrosymmetric superconductivity in multilayer systems. *J. Phys. Soc. Japan* **81**, 1–11 (2012).
- Sigrist, M. et al. Superconductors with staggered non-centrosymmetry. *J. Phys. Soc. Japan* **83**, 1–8 (2014).
- Clogston, A. M. Upper limit for the critical field in hard superconductors. *Phys. Rev. Lett.* **9**, 266–267 (1962).
- Sarma, G. On the influence of a uniform exchange field acting on the spins of the conduction electrons in a superconductor. *J. Phys. Chem. Solids* **24**, 1029–1032 (1963).
- Maeno, Y., Kittaka, S., Nomura, T., Yonezawa, S. & Ishida, K. Evaluation of spin-triplet superconductivity in Sr_2RuO_4 . *J. Phys. Soc. Japan* **81**, 1–29 (2012).
- Cavanagh, D. C., Shishidou, T., Weinert, M., Brydon, P. M. R. & Agterberg, D. F. Nonsymmorphic symmetry and field-driven odd-parity pairing in CeRh_2As_2 . *Phys. Rev. B* **105**, L020505 (2022).
- Möckli, D. & Ramires, A. Two scenarios for superconductivity in CeRh_2As_2 . *Phys. Rev. Res.* **3**, 023204 (2021).
- Yoshida, T., Sigrist, M. & Yanase, Y. Pair-density wave states through spin-orbit coupling in multilayer superconductors. *Phys. Rev. B* **86**, 1–6 (2012).
- Machida, K. Violation of the Pauli–Clogston limit in a heavy Fermion superconductor CeRh_2As_2 —duality of itinerant and localized 4f electrons. *Phys. Rev. B* **104**, 1–8 (2022).
- Sun, Z., Fogler, M. M., Basov, D. N. & Millis, A. J. Collective modes and terahertz near-field response of superconductors. *Phys. Rev. Res.* **2**, 1–19 (2020).
- Sauls, J. A. On the excitations of a Balian–Werthamer superconductor. *J. Low Temp. Phys.* **208**, 87–118 (2022).
- Bardasis, A. & Schrieffer, J. R. Excitons and plasmons in superconductors. *Phys. Rev.* **121**, 1050–1062 (1961).
- Böhm, T. et al. Balancing act: evidence for a strong subdominant d-wave pairing channel in $\text{Ba}_{0.6}\text{K}_{0.4}\text{Fe}_2\text{As}_2$. *Phys. Rev. X* **4**, 1–12 (2014).
- He, G. et al. Raman study of Cooper pairing instabilities in $\text{Li}_{1-x}\text{Fe}_x\text{OHFeSe}$. *Phys. Rev. Lett.* **125**, 1–6 (2020).
- Müller, M. A. & Eremin, I. M. Signatures of Bardasis–Schrieffer mode excitation in third-harmonic generated currents. *Phys. Rev. B* **104**, 1–11 (2021).

30. Müller, M. A., Volkov, P. A., Paul, I. & Eremin, I. M. Interplay between nematicity and Bardasis–Schrieffer modes in the short-time dynamics of unconventional superconductors. *Phys. Rev. B* **103**, 024519 (2021).
31. Uematsu, H., Mizushima, T., Tsuruta, A., Fujimoto, S. & Sauls, J. A. Chiral Higgs mode in nematic superconductors. *Phys. Rev. Lett.* **123**, 237001 (2019).
32. Allocca, A. A., Raines, Z. M., Curtis, J. B. & Galitski, V. M. Cavity superconductor-polaritons. *Phys. Rev. B* **99**, 020504 (2019).
33. Jost, D. et al. Indication of subdominant d-wave interaction in superconducting CaKFe4As4. *Phys. Rev. B* **98**, 020504 (2018).
34. Kretzschmar, F. et al. Raman-scattering detection of nearly degenerate s-wave and d-wave pairing channels in iron-based Ba0.6K0.6Fe2As2 and Rb0.8Fe1.6Se2 superconductors. *Phys. Rev. Lett.* **110**, 187002 (2013).
35. Anderson, P. W. Random-phase approximation in the theory of superconductivity. *Phys. Rev.* **112**, 1900–1916 (1958).
36. Rickayzen, G. Collective excitations in the theory of superconductivity. *Phys. Rev.* **115**, 795–808 (1959).
37. Möckli, D., Yanase, Y. & Sigrist, M. Orbitaly limited pair-density-wave phase of multilayer superconductors. *Phys. Rev. B* **97**, 144508 (2018).
38. Ptok, A. et al. Electronic and dynamical properties of CeRh2As2 layers and expected orbital order. *Phys. Rev. B* **104**, L041109 (2021).
39. Balian, R. & Werthamer, N. R. Superconductivity with pairs in a relative p wave. *Phys. Rev.* **131**, 1553–1564 (1963).
40. Nambu, Y. Quasi-particles and gauge invariance in the theory of superconductivity. *Phys. Rev.* **117**, 648–663 (1960).
41. Skurativska, A., Sigrist, M. & Fischer, M. H. Spin response and topology of a staggered-Rashba superconductor. *Phys. Rev. Res.* **3**, 033133 (2021).
42. Landaeta, J. F. et al. Field-angle dependence reveals odd-parity superconductivity in CeRh2As2. *Phys. Rev. X* **12**, 031001 (2022).
43. Boyack, R. & Lopes, P. L. Electromagnetic response of superconductors in the presence of multiple collective modes. *Phys. Rev. B* **101**, 94509 (2020).
44. Maiti, S. & Hirschfeld, P. J. Collective modes in superconductors with competing s- and d-wave interactions. *Phys. Rev. B* **92**, 094506 (2015).
45. Giuliani, G. & Vignale, G. *Quantum Theory of the Electron Liquid* (Cambridge University Press, 2005).
46. Binder, K. Theory of first-order phase transitions. *Rep. Prog. Phys.* **50**, 783–859 (1987).
47. Krumhansl, J. Landau models for structural phase transitions: are soft modes needed? *Solid State Commun.* **84**, 251–254 (1992).
48. Blazey, K. W., Miller, K. A., Ondris, M. & Rohrer, H. Antiferromagnetic resonance truncated by the spin-flop transition. *Phys. Rev. Lett.* **24**, 105–107 (1970).
49. Landau, L. D. & Lifshitz, E. M. *Statistical Physics* Vol. 5 (Elsevier, 2013).
50. Ahn, J. & Nagaosa, N. Theory of optical responses in clean multi-band superconductors. *Nat. Commun.* **12**, 1617 (2021).
51. Kamatani, T., Kitamura, S., Tsuji, N., Shimano, R. & Morimoto, T. Optical response of the Leggett mode in multiband superconductors in the linear response regime. *Phys. Rev. B* **105**, 094520 (2022).
52. Cea, T. & Benfatto, L. Signature of the Leggett mode in the A1g Raman response: From MgB2 to iron-based superconductors. *Phys. Rev. B* **94**, 1–14 (2016).
53. Maiti, S., Maier, T. A., Böhm, T., Hackl, R. & Hirschfeld, P. J. Probing the pairing interaction and multiple Bardasis–Schrieffer modes using Raman spectroscopy. *Phys. Rev. Lett.* **117**, 257001 (2016).
54. Maiti, S., Chubukov, A. V. & Hirschfeld, P. J. Conservation laws, vertex corrections, and screening in Raman spectroscopy. *Phys. Rev. B* **96**, 1–18 (2017).
55. Hardy, W. N., Bonn, D. A., Morgan, D. C., Liang, R. & Zhang, K. Precision measurements of the temperature dependence of λ in YBa2Cu3O6.95: strong evidence for nodes in the gap function. *Phys. Rev. Lett.* **70**, 3999–4002 (1993).
56. Feller, J. R., Tsai, C.-C., Ketterson, J. B., Smith, J. L. & Sarma, B. K. Evidence of electromagnetic absorption by collective modes in the heavy fermion superconductor UBe13. *Phys. Rev. Lett.* **88**, 247005 (2002).
57. Thiemann, M., Dressel, M. & Scheffler, M. Complete electrodynamics of a BCS superconductor with μeV energy scales: Microwave spectroscopy on titanium at mK temperatures. *Phys. Rev. B* **97**, 214516 (2018).
58. Bae, S. et al. Anomalous normal fluid response in a chiral superconductor UTe2. *Nat. Commun.* **12**, 2644 (2021).
59. Venderbos, J. W. F., Kozii, V. & Fu, L. Odd-parity superconductors with two-component order parameters: nematic and chiral, full gap, and Majorana node. *Phys. Rev. B* **94**, 180504 (2016).
60. Kibune, M. et al. Observation of antiferromagnetic order as odd-parity multipoles inside the superconducting phase in CeRh2As2. *Phys. Rev. Lett.* **128**, 057002 (2022).
61. Hackner, N. A. & Brydon, P. M. R. Bardasis–Schrieffer-like phase mode in a superconducting bilayer. arXiv:2306.16611 (2023).

Acknowledgements

We express our sincere thanks to Nico A. Hackner and P.M.R. Brydon for generously sharing their unpublished preprint on the BS mode⁶¹. We also thank Daniel Agterberg, Steven Kivelson, James Sauls, Hongki Min, Yunsu Jang, Jiho Jang, and Sungmo Kang for helpful discussions. S.B.C. was supported by the National Research Foundation of Korea (NRF) grants funded by the Korean government (MSIT) (NRF-2023R1A2C1006144, NRF-2020R1A2C1007554, and NRF-2018R1A6A1A06024977).

Author contributions

C.L. conducted the numerical calculation. C.L. and S.B.C. contributed to writing the manuscript.

Competing interests

The authors declare no competing interests.

Additional information

Supplementary information The online version contains supplementary material available at <https://doi.org/10.1038/s42005-023-01421-8>.

Correspondence and requests for materials should be addressed to Changhee Lee or Suk Bum Chung.

Peer review information *Communications Physics* thanks James Annett, Ilya Eremin, and the other, anonymous, reviewer(s) for their contribution to the peer review of this work.

Reprints and permission information is available at <http://www.nature.com/reprints>

Publisher's note Springer Nature remains neutral with regard to jurisdictional claims in published maps and institutional affiliations.



Open Access This article is licensed under a Creative Commons Attribution 4.0 International License, which permits use, sharing, adaptation, distribution and reproduction in any medium or format, as long as you give appropriate credit to the original author(s) and the source, provide a link to the Creative Commons license, and indicate if changes were made. The images or other third party material in this article are included in the article's Creative Commons license, unless indicated otherwise in a credit line to the material. If material is not included in the article's Creative Commons license and your intended use is not permitted by statutory regulation or exceeds the permitted use, you will need to obtain permission directly from the copyright holder. To view a copy of this license, visit <http://creativecommons.org/licenses/by/4.0/>.

© The Author(s) 2023